Tellus (1994), 46B, 16–32
Printed in Belgium – all rights reserved

TELLUS
ISSN 0280–6509

Laboratory measurements of mass transfer of carbon dioxide and water vapour for smooth and rough flow conditions

By F. J. OCAMPO-TORRES* and M. A. DONELAN[x], *National Water Research Institute, Canada Centre for Inland Waters, Burlington, Ontario, L7R 4A6, Canada*, N. MERZI, *Civil Engineering Department, Middle East Technical University, Ankara 06531, Turkey* and F. JIA, *Institute of Mechanics, Chinese Academy of Sciences, Beijing 100080, China*

(Manuscript received 20 January 1992; in final form 21 July 1993)

ABSTRACT

Mass transfer rates of carbon dioxide (CO_2) and water (H_2O) have been measured in a 32-m wind-wave tunnel, with a beach in the middle providing 2 sections of 16 m fetch. The wind speed (referred to 10 m) range explored was 1 to 24 m/s, covering a full range of aerodynamic conditions from smooth to fully rough. A pronounced minimum in the Dalton number for both CO_2 and H_2O is revealed. The minimum Dalton number, at wind speeds between 2 and 3 m/s, indicates a characteristic common point in the transfer mechanism for both gas and aqueous phase controlled constituents. This point corresponds to the occurrence of the first wind generated wavelets. At higher winds, the transfer rates of CO_2 increase more rapidly than those of H_2O, reflecting the increased importance of wave-generated turbulence for the ventilation of water phase limited compounds at the air-water interface.

1. Introduction

The transfer of mass, energy, and momentum across the air-water interface is a very important path in the global cycling system. Atmosphere and ocean act as a coupled thermodynamical system, in which the response of one phase to the forcing imposed by the other leads to variation in the transfer rates. The core of the problem of parameterizing the transfer process across the air-water interface is a phenomenological description of the way the resistance to transfer behaves. The resistance is largely in thin diffusive sublayers, on both sides of the interface. Gases of low solubility in water (like carbon dioxide) have their exchange controlled mainly in the water phase, while for those with high solubility or high reactivity the transfer is controlled in the air phase.

In spite of numerous laboratory and field investigations of CO_2 and moisture transfer processes, their behaviour is not yet satisfactorily understood. A complete phenomenological description is still lacking. For gases whose transfer is mainly controlled in the water phase a characteristic response of the gas transfer velocity to the wind speed has been noticed since the first laboratory experiments. A linear increase (for low wind speeds), and an abrupt enhancement (for higher) in both the gas transfer and friction velocities as a function of wind speed were reported from measurements in a small circular wind-wave tunnel (Jähne et al., 1979). The gas transfer velocity enhancement was initially associated with the influence of small capillary waves. Further work showed that a more appropriate quantity to parameterize the transfer velocity is the mean square slope of all wave components (Jähne et al., 1984).

* Present affiliation: CICESE, Departamento de Oceanografía Física, Km 107, Carretera Tijuana-Ensenada, Ensenada B. C., México.
[x] Corresponding author.

Empirical relations between wind speed and transfer velocity of carbon dioxide (CO_2) for instance, are already being used to estimate the CO_2 fluxes globally, from satellite wind data (Etcheto et al., 1991). Some measurements of air-sea exchange have been performed in rough and stormy seas (Watson et al., 1991). These are the first short term measurements of transfer velocity at sea in rough weather, and they support the wind dependence suggested by Liss and Merlivat (1986). However, the number of data points reported (only four) do not show much statistical significance. Therefore, more accurate transfer coefficients are needed in view of the sensitivity of the coupled system to CO_2 concentrations. Furthermore, it has been demonstrated that the exchange coefficients cannot be described solely by the wind field (Jähne, 1991). Wave-related roughness as an obvious characteristic of a wind disturbed water surface has to be incorporated in the transfer description (Kitaigorodskii and Donelan, 1984).

CO_2 transfer experimental results have been typically reported in terms of the actual mass transfer velocity K_{CO_2} (Liss, 1983). More recently, Jähne et al., (1987) considered the non-dimensional transfer velocity K_+ (normalized by the friction velocity in the water, u_{*w}) and found that it correlated well with the mean square slope of the waves (Jähne et al., 1987).

In the present work, for the case of CO_2 we also discuss a bulk transfer coefficient equivalent to the Dalton number in moisture transfer processes, which is the ratio of the transfer velocity to the wind speed. We therefore will refer to the exchange coefficients $\mathscr{D}_{CO_2}$ ($=K_{CO_2}/u$) and $\mathscr{D}_{H_2O}$ ($=K_{H_2O}/u$) as Dalton numbers for the CO_2 and H_2O transfer processes respectively. K_+ and $\mathscr{D}$ are related by the drag coefficient, C_D and the ratio of air and water densities.

There have been some suggestions indicating that the exchange coefficients (Dalton number for water vapour and Stanton number for heat, for instance) should vary with wind speed. The evaporation of water droplets in the near surface layer may be one of the causes for a significant enhancement of $\mathscr{D}_{H_2O}$. Statistical analysis of the problem of spray evaporation (Bortkovskiĭ, 1987) shows that the $\mathscr{D}_{H_2O}$ should increase by a factor of two from 9 to 18 m/s wind speed. However, no apparent variation in the Dalton number has been observed in field measurements. An average value of 1.2×10^{-3} has been reported (DeCosmo et al., 1988) for wind speeds ranging from 7 to 14 m/s, during the Humidity Exchange over the Sea Main Experiment (HEXMAX). During the same experiment, for wind speeds from 4 to 18 m/s other researchers (Smith and Anderson, 1988) determined that the average $\mathscr{D}_{H_2O}$ was also 1.2×10^{-3} with values varying from 0.8×10^{-3} to 2×10^{-3}.

Although much progress has been achieved in the last 20 years or so, the apparent differences between theoretical approaches and experimental results regarding the dependence of the exchange coefficients on the wind speed urges some further considerations. An appropriate parameterization of the transfer velocity as a function of wind and wave parameters as well as water turbulence information is urgently needed (Jähne et al., 1989). This goal can only be reached with a better knowledge of the physics of the transfer process in the near surface layers.

The objective of the present work is to advance our knowledge on the nature of the transfer process across the air-water interface, in particular of H_2O and CO_2. In addition to their importance in the global heat and water cycles, these gases make an interesting pair; the interfacial transfer of one (H_2O) being affected by turbulence in the air boundary layer, while the other is particularly sensitive to turbulent mixing beneath the surface. With an appropriate range of wind speeds, it will be shown that the mass transfer velocities and exchange coefficients (Dalton numbers) depend differently on roughness Reynolds number and on wave slope, and their dependence is associated with the different flow regimes and relevant physical phenomena involved in the transfer processes across the air-water interface. As the main resistance for the transfer of H_2O is in the air phase, while for CO_2 it is in the water phase, a joint investigation will possibly shed some light on the relative importance of the different physical mechanisms involved.

2. The experiments

2.1. The gas transfer flume

The Gas Transfer Flume (GTF) of the Hydraulics Laboratory at the National Water Research Institute (see Fig. 1) has a test section

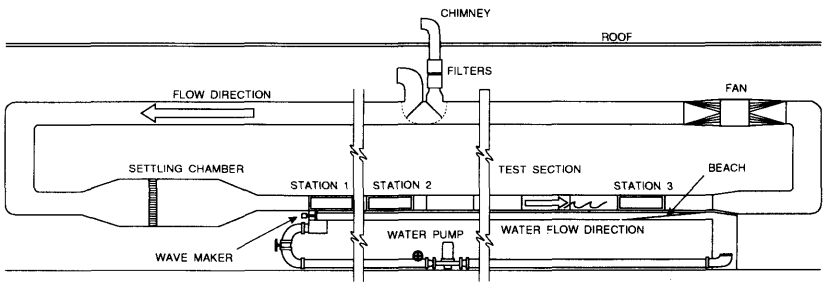

Fig. 1. Diagram of the gas transfer flume.

that is 32.2 m long and 0.76 m wide; the water depth can be up to 0.25 m while the air duct is 0.60 m high (Merzi et al., 1990). It may be operated either open ("ventilating mode") or closed ("circulating mode"). The experiments reported in this paper were conducted in the circulating mode; the flume is tightly closed and the air circulates continuously. A vaneaxial direct drive fan driven by a 25 hp variable speed motor is capable of delivering wind speeds up to 22.5 m/s measured on the centerline of the tunnel. The total air volume in the flume and return ducts is about 66 m^3, while the water volume is 10 m^3. A 2 m^3 tank ("tail box") at the downwind end of the test section and a smaller one at the upwind end ("head box") are connected by a 0.28 m diameter pipe which has an inline pump used to circulate and mix the water. The current induced by this pump in the test section may be varied continuously from 0 to 0.60 m/s.

There are three instrumented measuring stations in the GTF at 5.3 m, 14.5 m, and 29.7 m from the upwind end of the test section respectively, each with a profiling system. Sensors at the three stations used in this work are: (a) 0.2 mm diameter capacitance wires to measure wave height, and (b) Pitot tubes to measure wind speed. At station 1, a relative humidity sensor and thermistors for air and water temperature were also used. The sampling ports for CO_2 measurements in water and air and for water vapor were also at station 1. A differential, non-dispersive, infrared analyzer (NDIR (LI-6262, LiCOR)) was used for the measurements of CO_2 and H_2O. In this instrument the concentration measurements are based on the difference in absorption of infrared radiation passing through the sample and reference cells. At station 3, a laser slope gauge was used to measure the along-wind and cross-wind wave slopes.

An *inverted beach* was installed just upwind of station 2 in the GTF. The future use of the full flume length and more inverted beaches will enable us to generate various wind wave fields (with different mean square slopes) for a particular wind speed. The detailed analysis of the dependence of the mass transfer velocities on the mean square wave slope will be explored in a subsequent work. The inverted beach consisted of an aluminum plate with several layers of wire grids beneath. The plate is installed with a negative slope so that its upwind edge is about 5 cm above the still water surface and its downwind edge about 5 cm below. The plate spans the width of the test section and is 76 cm long. Waves approaching this beach loose their energy in the turbulence generated by interaction with the grid and are further damped by the rigid lid. This obstacle to waves divided the effective fetch in two for the experiments reported here, in such a way that the measurements at stations 2 and 3 correspond to a fetch of approximately 1 m and 16 m respectively, while those at station 1 are referred to the original 5.3 m fetch. Two main advantages of this type of beach are the following: (a) while it dissipates the wave energy, the wave breaking-generated turbulence does not enhance the mass transfer velocities as the contact with the air flow above is eliminated in the wave dissipation region, and (b) the flat aluminum plate facing the flume top does not appreciably obstruct the wind

flow in the sense that it is a smooth surface and the upwind edge is only 5 cm above the mean water level and the air duct is 62.5 cm high. Its effect is similar to a "tripping bar" used to initiate turbulence at the start of the fetch.

During the experimental runs to determine the mass transfer velocity of H_2O and CO_2, wave height η and reference wind speed u (measured at the air duct centerline approximately 30 cm above mean water level) were also measured at the three stations. The analog signals were digitized and recorded in a desktop computer (IBM 286) at 20 Hz. Water and air temperature were monitored and recorded at 1 Hz. During separate runs wave slopes were measured at station 3 and wind speed profiles were obtained at the three stations, in order to estimate the friction velocity u_* and the roughness scale z_0.

2.2. *Wind profiles and wave slope measurements*

Wind speed measurements as a function of height from the surface were carried out at the three stations for reference wind speeds up to about 16 m/s. The Pitot tube profiler systems sampled at levels 5 mm apart from the centerline downwards, at a sampling rate of 20 Hz for 10 s at each level. Simultaneously, wave height was measured at the three stations. The friction velocity u_* and the roughness scale z_0 were estimated at these three fetches. For the overall mass transfer measurements a better representation of the wind field is achieved by a fetch-averaged friction velocity, which is shown in Fig. 2 as a function of the measured wind speed.

Some runs were performed to measure wave slope at station 3. The mean square slope and the along-wind (η_x) and cross-wind (η_y) components are presented in Fig. 3. It is observed that the initial wavelets begin to appear at 2 m/s wind speed, and a sharp increase in the along-wind mean square slope occurs from 2 to 5 m/s wind.

2.3. *Experimental procedure for CO_2 transfer measurements*

Our experimental approach was to determine an overall mass transfer rate for the whole flume by closing the flume and monitoring the build-up of H_2O and CO_2 in the air phase as they are released by the enriched aqueous phase. The advantage of this approach is that it allows precise measurements with relatively slow instruments and avoids the sampling error inherent in point measurements. Since the water and air phases are very thoroughly mixed in their respective return ducts, the samples obtained at the upwind fetch are very good averages of the concentrations acheived at the end of the fetch some several seconds earlier. Of course, this approach requires an air and water tight flume, and extreme measures were employed in its construction to achieve this as far as possible. Periodic visual inspection provided assurance that the leakage of water was insignificant. Air leaks were isolated by "Helium sniffing" and repaired. The overall rate of air leakage was determined by pressurizing the flume to 15 cm H_2O and recording the rate of relaxation of the inside-outside differential pressure. The highest measured differential pressure across the flume, with the wind

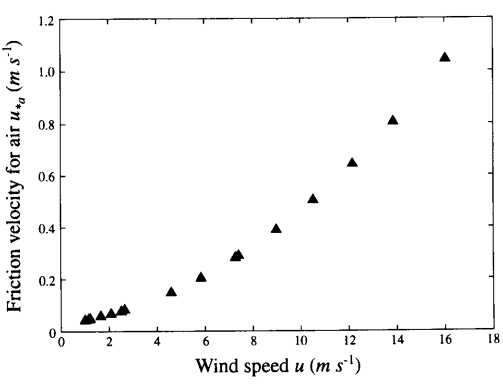

Fig. 2. Average air friction velocity u_{*a} versus the measured wind speed.

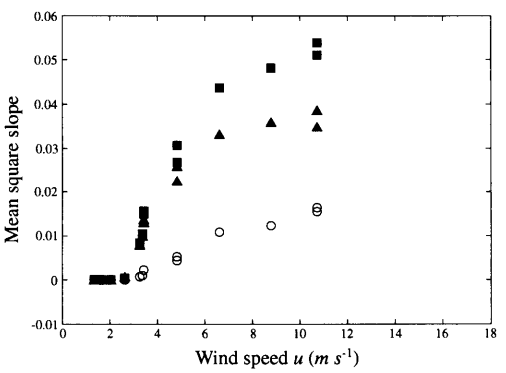

Fig. 3. Mean square slope measured at station 3 (■); along-wind component, η_x (▲); and cross-wind component, η_y (○).

speed at its upper limit, was 10 cm H_2O. Thus our pressure test was designed to yield a conservative estimate of the leakage. The observed pressure trend was 2.6 cm H_2O per hour corresponding to a leakage rate of 0.25% of the total volume of air per hour. The data reported here were based on 1000 s near the start of each run, so that the leakage rates are entirely negligible.

At the start of each constant wind speed run, the water was impregnated with CO_2 by bubbling into the tail box while the circulation pump was operated at a rather high speed (40 to 50 cm/s) thereby rapidly mixing the entire water mass. To avoid any CO_2 concentration build up in the air during this water impregnation procedure, the flume flaps were kept open so that air entered the flume from the laboratory and, after one circuit, exited to the atmosphere via the chimney (ventilating mode). The wind was maintained at low speed to keep the concentration of CO_2 and H_2O in the air at the ambient laboratory level as the initial condition. Input of CO_2 for about 15 min was observed to be sufficient for the concentration in the water to be near the upper limit of the NDIR analyzer. At this point, the source of CO_2 to the tail box was shut off, the water pump slowed down to about 10 cm/s, and once the water was well mixed (water phase CO_2 signal decreasing steadily for several minutes), the flume flaps were closed (circulating mode) and the wind was set to a specified speed, to begin the data gathering. After each run, the flume flaps were opened to evacuate the H_2O and CO_2-rich air. The subsequent input of CO_2 in the water represents the first step for the next run.

A timed valve was connected to the analyzer to allow sampling the air and water phase alternately with the same instrument, thereby avoiding cross calibration errors. The valve switched from air phase to water phase measurements (and vice versa) every two minutes.

The air phase CO_2 concentration (C_a) was given directly by the analyzer in ppm, as air from the flume is pumped out through a ceiling port into the analyzer sample cell at about 60–70 ml/min. Standard gas mixtures of CO_2 at 1000 ppm, 300 ppm and pure Nitrogen were used for calibration.

For the water phase CO_2 measurements, the following sparging method was employed. Water was piped out continuously from the tank, into the top of a 2 l glass column 110 cm high, and was pumped out from the bottom of the column, and returned to the tank, at a rate of 900 ml/min approximately. At the same time nitrogen was bubbled through the column at a rate of 60 ml/min, and the resultant mixture (N_2 and CO_2) went into the analyzer sample cell. The low N_2 flow allowed the gas bubbles sufficient time to equilibrate with the CO_2 in the water phase, at which point the measured CO_2 concentration in N_2 (C_g) was related to the CO_2 concentration in the water (C_w) by:

$$C_g = HC_w \tag{1}$$

(Yin and Hassett, 1986), where H is the non-dimensional Henry's Law parameter, which is related to the Henry's law constant for carbon dioxide (H_{CO_2}) through the universal gas constant R, and the water temperature T_w ($H = H_{CO_2}R(T_w + 273)$).

A high ratio of water flow to nitrogen flow prevents any appreciable depletion of the CO_2 in the sparging tower. This was checked previous to the experiments by allowing the CO_2 to come into equilibrium within the flume after leaving the wind on for several hours. Measurements of the CO_2 concentration in the water were made while varying the purge gas flow rate from 35 to 250 ml/min. For the water flow rate and column volume used in the experiments, any N_2 purging flow rate of 80 ml/min or lower gave a constant value, while for any higher flow the CO_2 concentration readings decreased.

The CO_2 analog signal was digitized and recorded at 1 Hz. The recordings began at the point the flaps were closed and the wind started. The length of the experiments varied between 1 and 3 h, depending on wind speed.

2.4. *Experimental procedure for H_2O transfer measurements*

The mass transfer of water vapour is two orders of magnitude faster than that for carbon dioxide, and the response of the NDIR analyzer was not sufficiently fast to track the rapid increase of water vapour in the air. Instead, the rate of change of water vapour concentration in the air phase was measured with a fast response (2 s) relative humidity sensor of the capacitance type (Vaisala "Humicap"). This sensor was calibrated at the

start and end of each run using the NDIR analyzer. Relative humidity (Humicap) and absolute water content (NDIR) signals were digitized and recorded in the computer at 1 Hz.

3. Data processing

Two examples of the original CO_2 data are shown in Fig. 4 as time series of measured concentration from the NDIR analyzer. The intake to the analyzer was switched back and forth between air and water (actually N_2 from the sparging tower) every 2 minutes. The upper envelope (that decreasing with time) corresponds to the CO_2 and N_2 mixture concentration (water phase concentration obtained by sparging with N_2, i.e., C_g) while the lower envelope represents the CO_2 concentration in the air (C_a). The actual CO_2 concentration in water (C_w) is calculated according to (1). Polynomial fitting to both air and water phase envelopes allows us to reconstruct the time series, filling the gaps due to the 2-min intermittency. Note that the initial 8 minutes are not taken into account for the polynomial fitting.

From Fig. 4 a time delay in the response for the water phase signal is readily apparent: the first two readings in CO_2 for the water phase are rather constant and lower than expected from extrapolating the envelope backwards in time. These first two readings of the water phase correspond to the concentration in the test section of the flume just before the wind was turned on. The delay of the water phase concentration relative to the air was introduced in our measurements as a consequence of the difference in time required for sampling the concentration in the two phases. From the volumes of the various vessels and discharge rates through them, the time required to register a change in concentration may readily be estimated. On the water side this is the sum of the residence time of the water in the glass sparging column (133 s), the time required for the CO_2 and N_2 mixture to reach the analyzer and replace the sample cell content (20 s), and the water circulating time through the return duct of the flume (263 s). Thus the total time on the water side is about 416 s. The corresponding time for the air-side concentration measurements is the sum of 0, 12 and $(107/u)$ (in s) (u is the reference wind speed in m/s). Thus, the total time required to register a change in concentration on the air side varied between 118 s and 19 s for the lowest and highest wind speeds (1.01 and 16.02 m/s) respectively. Consequently, one would expect the water concentration measurement to be delayed relative to the air by an amount:

$$\Delta t(s) = 404 - 107/u(m/s). \tag{2}$$

As a check on this calculation a shifting procedure was done in order to find the time delay between the air and water phase signals, using a mass balance condition as the criterion:

$$V_a C_a + V_w C_w = \text{constant}. \tag{3}$$

The sum of the CO_2 amount in air and water (a time series), will be most nearly constant (i.e., show a minimum standard deviation about its mean) when the correct delay is adopted and the

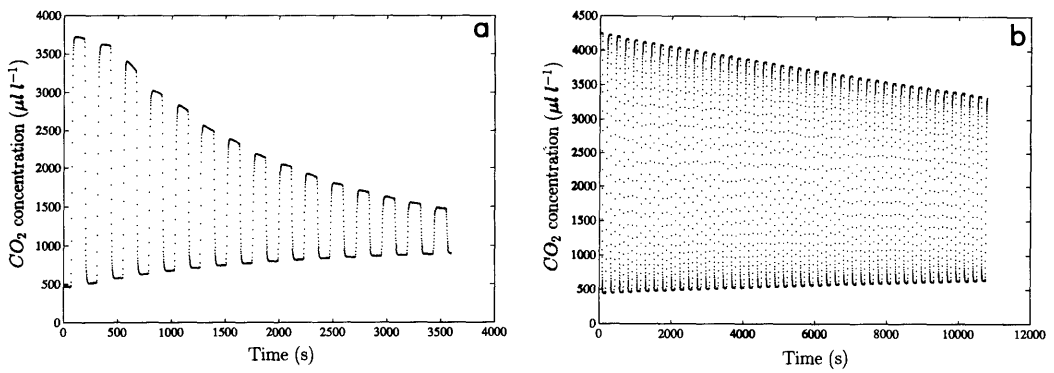

Fig. 4. Original time series of the CO_2 signal. The upper envelope corresponds to the measurements in the water phase (C_g), while the lower one to those in the air phase (C_a). The wind speed was (a) 16 m/s and (b) 2 m/s approximately.

mass balance is satisfied (Fig. 5). Typically mass balances better than 1% of total amount was achieved and the time delays were in general agreement with (2) at wind speeds above 5 m/s. At lower wind speeds the rate of change of concentration is too slow to permit an accurate assessment of Δt. Consequently, Δt was computed from (2) and used in all cases to shift the measurements of C_a and C_g to a common "in flume" time.

The estimation of the mass transfer velocity (K_{CO_2}) follows from either of:

$$\frac{\partial C_a}{\partial t}\frac{V_a}{A} = -\frac{K_{CO_2}}{H}(C_a - HC_w), \tag{4}$$

$$\frac{\partial C_w}{\partial t}\frac{V_w}{A} = -K_{CO_2}(C_w - C_a/H), \tag{5}$$

where A is the surface area of the air-water interface exposed to the wind (24.5 m^2), V_a and V_w are the total volumes of air and water (66 m^3 and 10 m^3), and $\partial C_a/\partial t$ and $\partial C_w/\partial t$ represent the time derivatives of the CO_2 concentrations in air and water. In terms of the direct concentration measurements of the NDIR analyzer, (4) and (5) may be written:

$$\frac{\partial C_a}{\partial t}\frac{V_a}{A} = -\frac{K_{CO_2}}{H}(C_a - C_g), \tag{6}$$

$$\frac{\partial C_g}{\partial t}\frac{V_w}{A} = -K_{CO_2}(C_g - C_a). \tag{7}$$

Thus, the ratio of the gradients of C_g and C_a directly yield the non-dimensional Henry's law parameter for CO_2 regardless of the accuracy of the calibration of the analyzer, provided only that its response is linear in CO_2 concentration. The mass transfer velocity may be determined directly from (7) and from (6) via H. Thus each realization of the experiment yields H and K_{CO_2}.

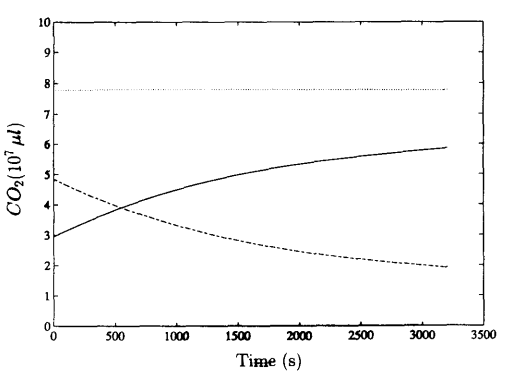

Fig. 5. Mass balance of CO_2 in the flume. The time series related to the amount in water (dashed line) has been shifted with respect to that for air (solid line). The total amount in the system remains constant (dotted line).

H is calculated from the ratio of the mean gradients (6) and (7) over the first 1000 s of each run. The corresponding values of H_{CO_2} are graphed in Fig. 6. At wind speeds over 7 m/s, the gradient estimates were particularly reliable (see below) and therefore we report the average value of H_{CO_2} as obtained from those runs: $H_{CO_2} = 0.0301 \pm 0.001$. This estimate of H_{CO_2} is then used to calculate H for each case based on its water temperature. The rate of change of concentration of CO_2 in air and water and the air-water difference are compared in Fig. 7.

Each run produces a time series of $\partial C_a/\partial t$, $\partial C_g/\partial t$ and of $(C_g - C_a)$. The 3rd order polynomial fit to these, allows us to calculate K_{CO_2} as a time series. A constant value of K_{CO_2} in (6) and (7) corresponds to a straight line through the origin in Fig. 7. As the experiment progresses the points advance along the line towards the origin. The larger gradients at the start of each run yield more accurate estimates of K_{CO_2}. Therefore, using least squares, we fitted such a line to the first 1000 s of each run.

A measure of the conformity of the data to a constant K_{CO_2} is the % variance of $\partial C/\partial t$ of the first 1000 points "explained" by the fitted straight line through the origin. This is graphed in Fig. 8. At wind speeds above 7 m/s, both air and water phase measurements are in agreement with (6) and (7) with 80% explained variance. At lower wind speeds the agreement is not as good and cases with less than 50% explained variance were rejected. There were 5 of these, all water-side measurements.

The principal resistance to transfer of CO_2

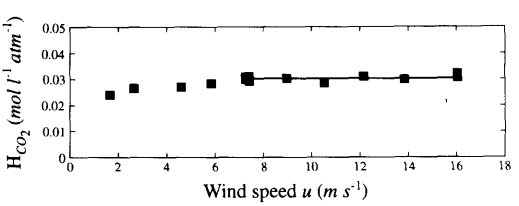

Fig. 6. Estimates of Henry's law constant for CO_2 at different wind speeds.

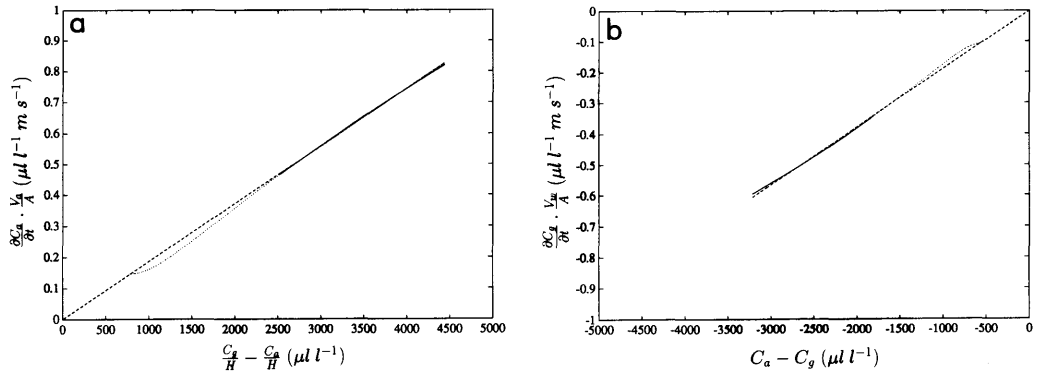

Fig. 7. Rate of change of the CO_2 concentration in (a) air and (b) water versus the concentration difference for an experimental run with 16 m/s wind (dotted line). The slope of the fitted line through the origin (dashed line) represents the mass transfer velocity. The fitting is done in the first 1000 seconds of each experimental run (shown as a solid line).

across the air-water interface occurs in the thin (O(0.1 mm)) diffusive boundary layer beneath the surface. Consequently, any sources of turbulence in the water near the surface can cause an enhancement of the mass transfer rate. One possible unwanted source of such turbulence is that produced by the pump-driven current of 10 cm/s. Our method depends on circulating and mixing both air and water phases, so that some imposed current is unavoidable. In order to determine the effect of the current on the measurements of K_{CO_2}, several runs were performed at a fixed wind speed and various current speeds. The wind speed chosen was 3 m/s because the mass transfer velocity has a fairly flat minimum in this region (Fig. 10). Fig. 9 shows the effect of water current speed on mass transfer velocity. Separate regression lines to the air and water phase measurements yield estimates of the difference between no current and the operating current of 10 cm/s. This (average) difference (3.1×10^{-6} m/s) is taken to be the pump-induced enhancement of K_{CO_2} and is subtracted from all the estimates of K_{CO_2} derived from (6) and (7). In the worst case, this correction is 32%. The corrected values are our estimates of K_{CO_2}. They are tabulated in Tables 1 and 2 and, after adjustment to a common Schmidt number of 600, graphed in Fig. 10.

The mass transfer velocity for water is estimated from:

$$\frac{\partial Q}{\partial t}\frac{V_a}{A} = -K_{H_2O}(Q - Q_{sat}). \quad (8)$$

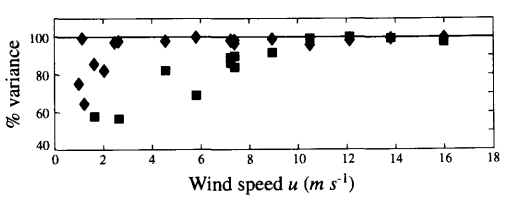

Fig. 8. Per cent of variance of $\partial C/\partial t$ of the first 1000 points "explained" by the fitted straight line through the origin. Estimates from $\partial C_w/\partial t$ are indicated by (■), and from $\partial C_a/\partial t$ by (◆).

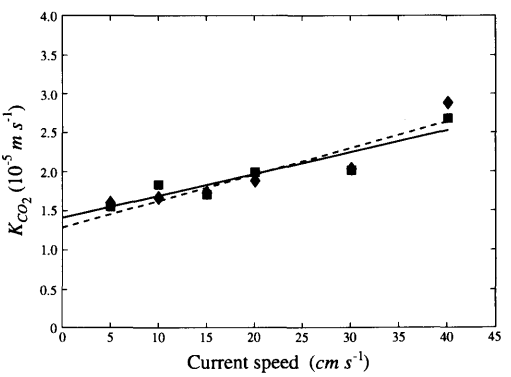

Fig. 9. Mass transfer velocity versus current speed at a fixed wind speed of 3 m/s. Separate regression lines to the air (dashed line) and water (solid line) phase measurements yield estimates of the difference between no current and the operating current of 10 cm/s. K_{CO_2} estimated from the rate of change of concentration in water is (■), and from the rate of change in concentration in air is (◆).

Table 1. *Summary of CO_2 experiments session I, April 1991*

Run	t [s]	T_a [°C]	T_w [°C]	$\bar{u}_1$ [m/s]	$\bar{u}_2$ [m/s]	$\bar{u}_3$ [m/s]	u [m/s]	$[K_{CO_2}]_a$ [m/s]	$[K_{CO_2}]_w$ [m/s]	u_{*a} [m/s]
44	3600	23.15	20.55	—	16.40	15.63	16.02	0.183×10^{-3}	0.186×10^{-3}	1.046
47	3600	23.61	21.46	—	16.39	15.64	16.02	0.180×10^{-3}	0.188×10^{-3}	1.046
69	3600	23.78	21.75	13.26	14.49	13.75	13.83	0.151×10^{-3}	0.148×10^{-3}	0.807
48	3600	23.95	21.59	—	12.59	11.67	12.13	0.113×10^{-3}	0.116×10^{-3}	0.644
51	3600	23.21	21.73	8.95	9.35	8.59	8.96	0.724×10^{-4}	0.724×10^{-4}	0.389
53	5400	23.37	21.86	6.09	6.00	5.38	5.83	0.370×10^{-4}	0.346×10^{-4}	0.204
66	5400	24.15	21.79	5.04	4.59	4.10	4.58	0.248×10^{-4}	0.217×10^{-4}	0.148
59	10800	23.00	20.21	3.51	2.45	1.96	2.64	0.830×10^{-5}	0.691×10^{-5}	0.081

The specific humidity Q (g/kg) is obtained from the relative humidity signal (r in %) according to:

$$Q=\frac{6.22e_s r}{p-e_s r(0.00378)}, \tag{9}$$

where e_s is the saturation vapour pressure (mb):

$$e_s=6.11\exp\left[\frac{L_v}{(R\times273)}\frac{T_a}{(T_a+273)}\right], \tag{10}$$

and p is the pressure in mb, L_v is the latent heat of vapourization of water, and T_a is the air temperature (°C). The saturated value for specific humidity Q_{sat} is estimated from the average of the last (constant) portion of the record from the NDIR analyzer absolute water content signal, once converted from mmol/mol to g/kg. Note that Q_{sat} is used instead of the surface value Q_{sfc}. The reason is that we do not know the surface temperature (cool skin) T_{sfc}, and we assume that Q_{sat} is its corresponding value. A running average (61 points) is applied to the specific humidity time series Q previous to the estimation of K_{H_2O} which follows from a regression analysis in accordance with (8). In Fig. 11 typical time series of Q (and its smooth version) and of the water content from the NDIR analyzer are shown. The slow response of the analyzer in comparison to Q is clearly noticeable. The runs lasted long enough however, for the signal to reach an equilibrium level, and that absolute quantity is considered to be the saturation value. The relation between the time derivative of the smoothed water content and the difference between the smoothed water content at a specific time and its saturation value is shown in Fig. 12. The slope of the fitted straight line yields the mass transfer velocity for water K_{H_2O}. These are graphed in Fig. 13 versus the reference wind speed.

Table 2. *Summary of CO_2 experiments session II, May–Jun 1991*

Run	t [s]	T_a [°C]	T_w [°C]	$\bar{u}_1$ [m/s]	$\bar{u}_2$ [m/s]	$\bar{u}_3$ [m/s]	u [m/s]	$[K_{CO_2}]_a$ [m/s]	$[K_{CO_2}]_w$ [m/s]	u_{*a} [m/s]
151	7200	24.62	20.18	1.03	1.05	0.95	1.01	0.745×10^{-5}	—	0.047
149	7200	26.38	21.58	1.05	1.09	1.36	1.17	0.665×10^{-5}	—	0.047
159	7200	23.58	20.42	1.18	1.25	1.23	1.22	0.901×10^{-5}	—	0.048
148	7200	25.74	21.20	1.39	1.69	1.87	1.65	0.766×10^{-5}	0.547×10^{-5}	0.057
146	7200	24.48	20.74	1.83	2.05	2.31	2.06	0.665×10^{-5}	—	0.066
144	5400	23.60	18.51	2.34	2.52	2.61	2.49	0.819×10^{-5}	—	0.077
166	5400	24.62	21.62	7.04	7.58	7.14	7.25	0.514×10^{-4}	0.522×10^{-4}	0.281
162	5400	24.08	21.19	7.04	7.61	7.17	7.27	0.515×10^{-4}	0.512×10^{-4}	0.282
164	5400	23.02	20.90	7.18	7.75	7.27	7.40	0.537×10^{-4}	0.518×10^{-4}	0.289
160	5400	23.58	20.76	7.17	7.73	7.29	7.40	0.518×10^{-4}	0.530×10^{-4}	0.289
165	3600	23.63	21.20	10.10	10.98	10.41	10.50	0.949×10^{-4}	0.892×10^{-4}	0.505

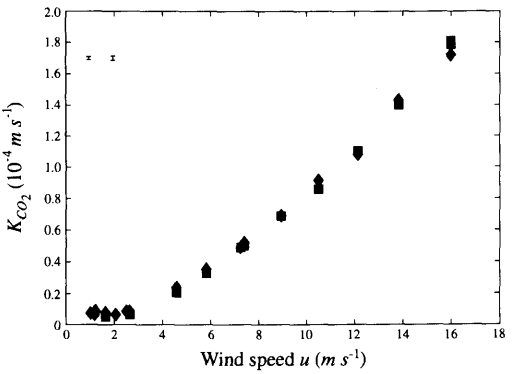

Fig. 10. Mass transfer velocity for CO_2 (K_{CO_2}), versus wind speed, as estimated from the rate of change of the concentration in water (■) or in air (◆). The measurements have been corrected to "zero imposed water current" and are adjusted to a Schmidt number of 600. The standard errors for the four experiment runs for a wind speed of about 7.3 m/s are shown in the upper left corner; water on the left, air on the right.

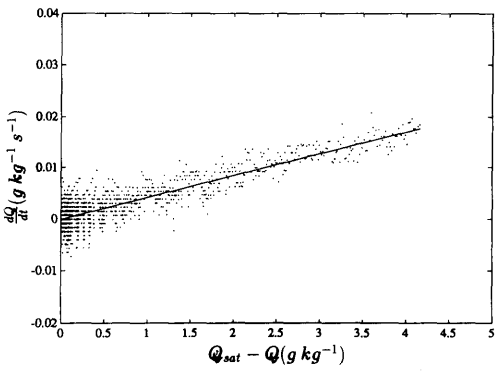

Fig. 12. A typical example of $\partial Q/\partial t$ (smoothed) versus $Q_{sat} - Q$ (smoothed) as the experimental run progresses. The slope of the fitted straight line is proportional to the mass transfer velocity for water vapor K_{H_2O}.

4. Results

A summary of the experimental runs carried out during two different sessions to measure the CO_2 mass transfer velocity (K_{CO_2}) is given in Tables 1 and 2. The average air and water temperature were 24°C and 21°C respectively. During runs number 44, 47 and 48, the Pitot tube at station 1 was not functioning.

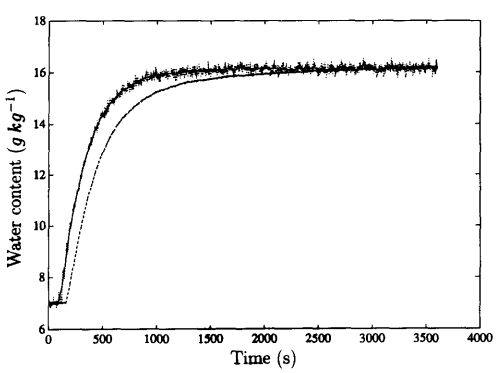

Fig. 11. Time series of the water content signal (g/kg) from the NDIR analyzer (dashed line), and from the relative humidity sensor via eq. (9) (dotted line) and its smooth version (solid line).

The wind-speed dependence of the CO_2 transfer velocity seems to be stronger than linear as can be seen in Fig. 10, where the wind speed reported is an average over the fetch obtained from the three Pitot tubes at approximately 30 cm above mean water level. In this figure, the standard error is also shown for the four independent runs carried out at about 7.3 m/s wind speed. This is a clear indication of the between-runs reproducibility of these laboratory measurements. The results for the mass transfer measurements of H_2O are summarized in Table 3. The wind speed dependence of the water transfer velocity K_{H_2O} is clearly observed in Fig. 13. K_{H_2O} increases with wind speed for all the range of speeds considered, while for the case of CO_2 below 3 m/s, its transfer velocity remains practically constant.

Clearly distinguishable is an increase in the transfer velocity of CO_2 associated with the onset of initial waves, at a wind speed of about 3 m/s. However, no abrupt enhancement is observed at the higher wind speeds, that could possibly be related to active breaking of gravity waves although some breaking occurred at wind speeds above 10 m/s at the end of the fetch. As might be expected K_{H_2O} shows no sudden change associated with the onset of initial waves.

These differences between water phase and air phase limited compounds are expected since the micro breaking of small waves has a pronounced effect on "ventilating" the water side diffusive sublayer and a much smaller effect on the turbulence

Table 3. *Summary of H_2O experiments, April–May 1991*

Run	t [s]	p [kPa]	T_a [°C]	T_w [°C]	$\bar{u}_1$ [m/s]	$\bar{u}_2$ [m/s]	$\bar{u}_3$ [m/s]	u [m/s]	K_{H_2O} [m/s]	u_{*a} [m/s]
84	10800	100.97	23.86	20.71	0.92	1.18	—	1.05	0.0020	0.039
85	7200	100.95	23.93	20.76	1.15	1.71	1.00	1.28	0.0032	0.049
92	7200	100.99	23.94	20.01	1.28	1.43	1.60	1.44	0.0035	0.053
88	5200	100.14	23.36	18.68	1.40	1.56	1.77	1.57	0.0037	0.055
86	7200	100.40	20.91	18.15	1.93	2.26	1.75	1.98	0.0040	0.064
87	7200	100.25	22.13	18.39	2.43	2.66	2.17	2.42	0.0045	0.075
81	7200	100.18	23.72	21.12	2.53	2.96	2.44	2.64	0.0049	0.081
80	7200	99.46	24.63	21.37	3.44	3.71	3.42	3.52	0.0070	0.109
79	7200	99.82	23.85	21.11	4.11	4.59	4.01	4.24	0.0084	0.134
83	3600	100.20	24.13	21.41	4.93	5.41	4.93	5.09	0.0115	0.170
78	3600	99.89	23.49	20.09	5.98	6.51	5.95	6.15	0.0146	0.220
77	1800	99.89	23.31	19.82	7.77	8.45	7.79	8.01	0.0199	0.326
76	3600	99.96	22.80	19.55	9.57	10.54	9.73	9.95	0.0239	0.462
75	1800	100.04	21.93	18.50	11.30	12.53	11.72	11.85	0.0300	0.619
74	1800	100.04	21.53	18.19	12.93	14.40	13.66	13.66	0.0379	0.791
73	1200	100.04	21.55	17.79	14.47	16.15	15.52	15.38	0.0499	0.973

in the air. Of course, the turbulence produced by the sheared wind drift current is also effective in enhancing K_{CO_2}. The key question is to determine the balance of these two sources of turbulence (shear generated and wave breaking) on establishing the mass transfer rate of water phase limited compounds. We will return to this later.

For purposes of calculating fluxes at the air-water interface based on meteorological data, a bulk parameterization of the transfer rates in terms of wind speed is usually most convenient. In Figs. 14 and 15, we show the bulk transfer coefficients (or Dalton numbers) based on the reference wind speed. In both cases, a minimum is observed for wind speeds between 2 and 3 m/s. High Dalton numbers for low wind speed correspond to the flow over a smooth surface. A clear increase in $\mathscr{D}_{CO_2}$ with wind speed is observed for higher wind speeds. $\mathscr{D}_{H_2O}$, on the other hand, shows almost no change in the wind speed range of 6 to 12 m/s, and increases again above that speed, possibly because of spray evaporation. The relative minimum is shown to be much deeper for CO_2 than that observed for H_2O. $\mathscr{D}_{CO_2}$ varies over a factor of 4 in the wind speed range observed, while $\mathscr{D}_{H_2O}$

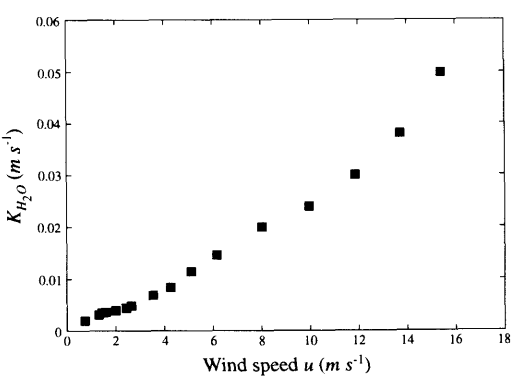

Fig. 13. Mass transfer velocity for H_2O (K_{H_2O}) versus the reference wind speed.

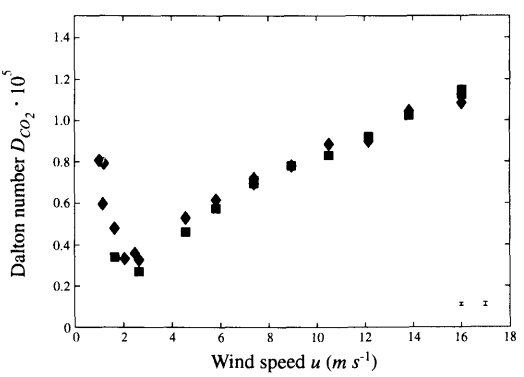

Fig. 14. Dalton number $\mathscr{D}_{CO_2}$ for the CO_2 transfer process (at $Sc = 600$) versus wind speed. The standard errors for the four experiment runs for a wind speed of about 7.3 m/s are shown in the lower right corner; water on the left, air on the right.

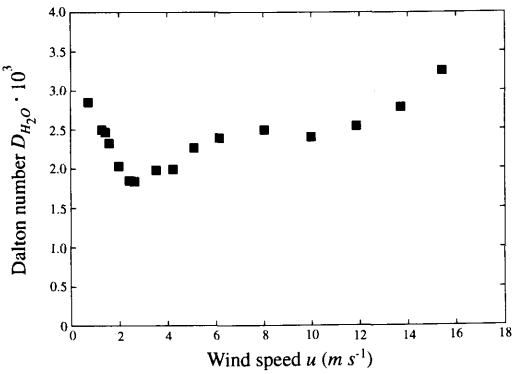

Fig. 15. Dalton number $\mathscr{D}_{H_2O}$ for the H_2O transfer process versus wind speed.

varies by a factor of 2. Such a detailed dependence of bulk gas transfer coefficients with wind speed is revealed from experimental results for the first time.

A clear association can be made between the increase in surface roughness as indicated by the mean square slope (see Fig. 3), and the increase in $\mathscr{D}_{CO_2}$, for wind speeds of about 3 m/s. The $\mathscr{D}_{CO_2}$ values obviously reflect the influence of other factors besides the mean square slope and wind speed, such as the breaking of the long gravity waves in the system, which occurs at the end of the fetch for wind speeds of about 10 m/s or higher. No sharp transition in $\mathscr{D}_{CO_2}$ is seen at the speed where wave breaking begins in the tank. Circular tanks generate a more uniform wave field and so the change in wind speed from non-breaking to breaking waves may be quite abrupt. By contrast, in these measurements an increase in the wind speed simply shortens the fetch where wave breaking starts, so more and more area is subject to breaking as the speed increases. Consequently, a smooth increase of $\mathscr{D}_{CO_2}$ with wind speed is observed.

5. Discussion

5.1. *Comparison with mass transfer velocities from other experiments*

There is a considerable number of laboratory measurements of the transfer velocity of gases in general. However, there are not many where specifically CO_2 transfer has been measured (Jähne et al., 1987; Liss, 1983). Transfer velocity estimated with tracers other than CO_2 is usually reported as corrected for a tracer with Schmidt number equal to 600, the equivalent to that of CO_2 at a temperature of 20°C. Since the Schmidt number dependence of the transfer process is not satisfactorily understood and the effect of the wave field in regulating the transfer process has been proven to be important (Jähne, 1991), we decided to compare our measurements of K_{CO_2} with only those obtained using CO_2 directly in other experiments, and correspondingly those of K_{H_2O} with measurements of the moisture transfer process.

In Fig. 16, the results of evaporation measurements made from a small tank (4.50 m × 0.30 m × 0.10 m) placed in a wind tunnel (Liss, 1973), are compared to the values of K_{H_2O} obtained in our experiments. Liss's wind speeds were measured at 10 cm height and our results are also shown against wind speed extrapolated to that height. While it is true that our flume is larger than Liss's tank, and therefore a more developed wave field is simulated, the trend of K_{H_2O} to increase with wind speed is quite similar in both cases. At low and moderate wind speed, when no spray or bubbles are yet present, the transfer process is governed by the behaviour of the physical properties in the gas phase. The differences encountered (Liss's values are about 15% higher than ours) between these two experiments must be largely due to the increased turbulence induced by the small tank installed in the tunnel, enhancing the evaporation process.

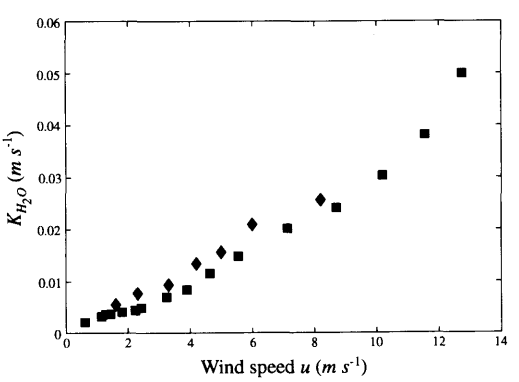

Fig. 16. Comparison of the mass transfer velocity K_{H_2O} with the results from another experiment. The wind speed is measured or extrapolated to 10 cm height. Present work (■), and from Liss (1973) (◆).

A comparison of the mass transfer velocity for CO_2 reported from experiments in different small tanks (Kanwisher, 1963; Hoover and Berkshire, 1969; Liss, 1973), with those obtained in the present work is shown in Fig. 17. It is not surprising that the less developed wind wave field generated in the small tanks affects the measurements resulting in lower values of K_{CO_2}. This is noticeable for wind speed higher that 4 m/s (the exception is the result from Kanwisher). Although microscale breaking may be present even during the early stages of wave development, and may disrupt the diffusive sublayer below the interface, it gets more frequent and important as the waves develop further and as the wind gets stronger. These results stress the importance of the wave field on the transfer process, and the fact that tank dimensions must be properly considered when making intercomparisons among different laboratory experiments.

The results of one set of experiments on CO_2 transfer (Broecker et al., 1978) carried out in a tank with fetch slightly larger than that of the GTF are presented in Fig. 18 (the size of their tank was 18 m × 1.0 m × 0.5 m). Although the air and water temperature were about 10°C, for which the Schmidt number of CO_2 is approximately 1000, we include these results since they are the only previous measurements of K_{CO_2} in a large wind and wave tunnel. Therefore, the K_{CO_2} values have been corrected to a Schmidt number of 600. Their results are consistently higher than ours, possibly due to the longer fetch (18 m) for the waves to develop. The values of K_{CO_2} measured in a small circular tank (Jähne et al., 1979) are also shown in this figure. Since circular flumes can presumably be considered to have unconfined fetch, the wave field is more developed and homogeneous, therefore higher transfer velocities are expected. The sharp increase in K_{CO_2} for winds higher than 8 m/s is associated with a sudden transition from a very smooth flow regime, with the presence of a surface film inhibiting the appearance of waves, to a very rough flow regime once the waves are generated and grow continuously to reach a steady and homogeneous state (Jähne et al., 1979). Linear flumes inherently simulate a fetch dependent wave field and average properties are responsible for the transfer measured. Therefore, no abrupt enhancing of K_{CO_2} is observed in our experiments and our measured transfer velocities are lower than those reported by Jähne et al. (1979) for winds higher than 8 m/s.

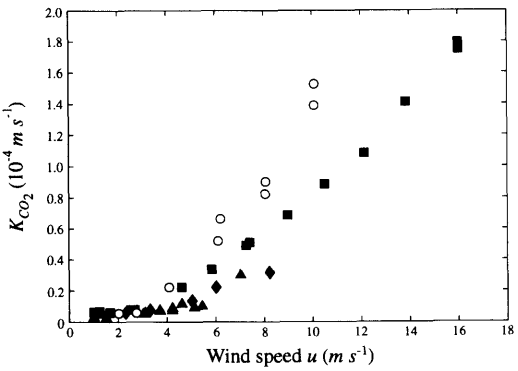

Fig. 17. Comparison of the mass transfer velocity K_{CO_2} with the results from other experiments in small tanks. Present work (■), from Liss (1973) (◆), Kanwisher (1963) (○), and Hoover and Berkshire (1969) (▲).

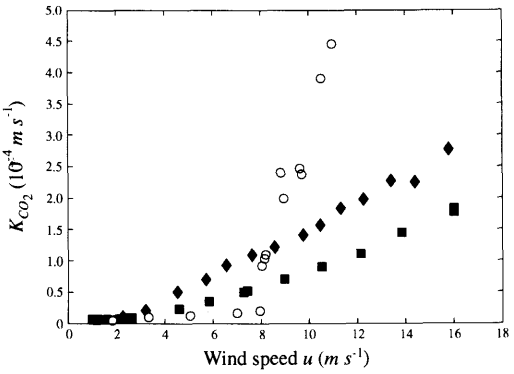

Fig. 18. Comparison of the mass transfer velocity K_{CO_2} with the results from other experiments in large linear, and small circular tanks. Present work (■), from experiments of Broecker et al. (1978) in a 18 m linear tank, corrected to a Schmidt number of 600 (◆), and from experiments of Jähne et al. (1979) in a circular flume (○).

5.2. *Comparison of mass transfer rates of CO_2 and H_2O*

The wave field influence on the water side controlled gas transfer process has been recognized from previous experiments (Broecker et al., 1978; Jähne et al., 1979). It is clear that the mass transfer velocities cannot be parameterized solely by the wind speed. In this section, we discuss our results in the context of the non-dimensional mass

transfer rate and its possible association with the characteristics of the wind and wave fields present in the experiments.

In order to compare the mass transfer rates of gases that are limited in different phases, we seek to reduce them to a common reference state. The physical characteristics that are important to the problem are: the viscosity of air and of water (ν_a and ν_w); the Schmidt numbers of H_2O and CO_2 in their limiting phases (air and water respectively). Two of the important flow characteristics are: the friction velocity in both air (u_{*a}) and water (u_{*w}), and the mean square slope of the waves. To calculate u_{*w} from the measured u_{*a} values, we assume that the stress is continuous across the interface. The mass transfer velocities of H_2O and CO_2 are normalized by the friction velocity in the corresponding limiting phase; u_{*a} and u_{*w}, respectively:

$$[K_+]_{H_2O} = K_{H_2O}/u_{*a}, \tag{11}$$

$$[K_+]_{CO_2} = K_{CO_2}/u_{*w}. \tag{12}$$

Then the non-dimensional transfer rates are reduced to their equivalent value for Sc = 600. The Schmidt number dependence of CO_2 on temperature was taken from Jähne et al. (1987b) and a Schmidt number of 0.6 was used for H_2O. For wind speeds below 2 m/s, mean square slopes were below the resolution of the laser slope gauge ($\approx 10^{-6}$) and these conditions were considered to be smooth. Following Jähne et al. (1987a), we corrected the K_{CO_2} values using a Schmidt number exponent of -0.7. For all higher wind speeds an exponent of -0.5 was used. For CO_2, the corrections are less than 9%, since we kept the water temperature in the range of 18.5°C to 21.9°C corresponding to a Schmidt number variation of 635 to 532. These corrections are appropriate for CO_2, whose transfer properties are determined by the turbulence in the water near a free surface. The transfer of H_2O, on the other hand, is determined by the near-surface turbulence in the air and the dense water surface is more appropriately viewed as a solid wall than as a free surface. For smooth flow over a solid wall Shaw and Hanratty (1977) report a Schmidt number dependence of -0.704, while for a rough solid wall Dawson and Trass (1972) determined a Schmidt number dependence of -0.58. These exponents are applied to all the K_{H_2O} data and the corrected results are indicated separately in Fig. 19. The abscissa is the appropriate roughness Reynolds number: in the air for H_2O and in the water for CO_2.

$$Re_{*a} = \frac{z_0 u_{*a}}{\nu_a}, \tag{13}$$

$$Re_{*w} = \frac{z_0 u_{*w}}{\nu_w}. \tag{14}$$

The Shaw and Hanratty (1977) and Dawson and Trass (1972) results are shown in their appropriate Reynolds number ranges. Generally speaking the $[K_+]_{H_2O}$ values are not in agreement with the empirical results from mass transfer at solid walls, being a factor of 2 lower at low Reynolds numbers (compare filled circles with the solid line). At high Reynolds numbers, our results intersect the results of Dawson and Trass but are not in agreement with their $Re_*^{-1/4}$ dependence (compare open circles with the dashed line). It is

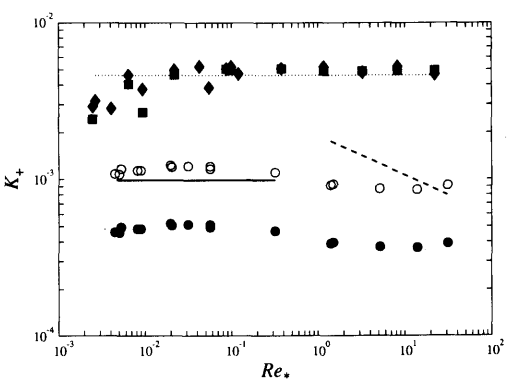

Fig. 19. Mass transfer velocity for CO_2 and H_2O, normalized with the water and air (respectively) friction velocities, versus the roughness Reynolds number Re_{*w} and Re_{*a} in water and air (respectively). $[K_+]_{CO_2}$ was estimated using either the rate of change of concentration in air (◆) or in water (■). The fit to the results of Jähne et al. (1987a) is indicated by the dotted line. For comparison $[K_+]_{H_2O}$ has been adjusted to a Schmidt of 600 using exponents of -0.704 (●) and -0.58 (○). The solid wall results of Shaw and Hanratty (1977) for smooth flow (solid line) and of Dawson and Trass (1972) for rough flow (dashed line) are also shown.

apparent that measurements of mass transfer at solid walls do not yield good predictors of the mass transfer of air phase limited gases at the air-water interface. Not suprisingly, the solid wall results are even less accurate for the water phase limited gases. Our measurements indicate transfer rates of CO_2 about a factor of 3 faster than the solid wall estimates, with no indication of a decrease of normalized mass transfer rate at high Reynolds numbers.

Jähne et al. (1987a) have demonstrated this enhancement over the solid wall results. They found that for a free surface the normalized mass transfer rate of water phase limited compounds is well represented by $0.11Sc^{-0.5}$ (dotted line). Our results corroborate theirs and also show the inadequacies of the solid wall results in predicting transfer rates of air phase limited compounds at the air-water interface.

Clearly the modelling of air-water mass transfer requires new insights and many careful measurements to establish the Schmidt number, Reynolds number and wave slope dependencies of the normalized mass transfer rate of both air phase and water phase limited compounds. We are continuing to explore these matters in both laboratory and field experiments.

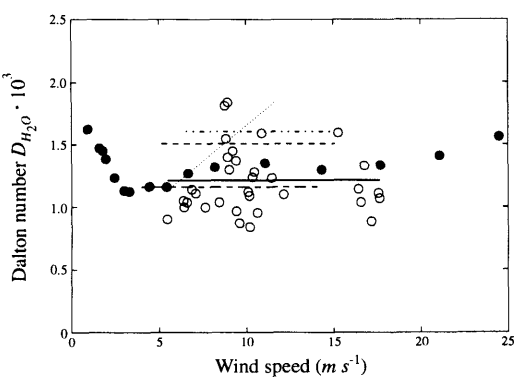

Fig. 20. Comparison of the Dalton number $\mathscr{D}_{H_2O}$ with the results from other experiments. Present work adjusted to the 10 m reference height (●), from Smith and Anderson (1988) during HEXMAX (○), the solid line is the HEXMAX average. From Garratt and Hyson (1975) (dashed-double dotted), Francey and Garratt (1979) (dashed line), Anderson and Smith (1981) (dotted line), and Large and Pond (1982) (dashed-dotted line).

5.3. Comparison of $\mathscr{D}_{H_2O}$ with oceanic measurements

In order to make a proper comparison with some of the results from experiments at sea, the values of $\mathscr{D}_{H_2O}$ have been adjusted to a height of 10 m and are presented in Fig. 20 along with some of the results reported in the literature. The characteristic wind speed dependence of $\mathscr{D}_{H_2O}$ from the experiments is still observable from the $\mathscr{D}_{H_2O}$ values adjusted to 10 m height, although it is less pronounced. The latest HEXMAX results are believed to support a constant $\mathscr{D}_{H_2O}$, proposed some years ago (Smith, 1989) on the basis of the analysis of the results of a number of laboratory and field experiments. $\mathscr{D}_{H_2O}$ estimates from HEXMAX (Smith and Anderson, 1988) for a range of wind speeds between 4 and 18 m/s are shown scattered between approximately 0.8×10^{-3} and 2.0×10^{-3} about an average = 1.2×10^{-3} (see Fig. 20), even though the drag coefficient was found to increase significantly with the wind speed. The results from other experiments as well as those from HEXMAX are scattered about our $\mathscr{D}_{H_2O}$ values. The averages are shown in the figure.

It is apparent that our laboratory measurements are consistent with field estimates of $\mathscr{D}_{H_2O}$. However, the scatter in the field measurements is such that the details of the variations of $\mathscr{D}_{H_2O}$ are completely obscured. It may well be that field measurements, such as those reported in Fig. 20, may be inherently incapable of the precision required to reveal the underlying source of variation of the Dalton numbers.

6. Acknowledgments

We thank the members of the National Water Research Institute who contributed to the experimental work of this project. In particular, the assistance of D. Beesley, G. Voros and M. Alaée was very valuable. F. J. Ocampo-Torres was a Visiting Fellow while this work was carried out and he thanks the personnel of the Institute for their hospitality. He was also supported by CONACyT (Mexico) under project 1109-T9201 during the final part of the manuscript preparation. The helpful comments of the reviewers are also acknowledged.

REFERENCES

Anderson, R. J. and Smith, S. D. 1981. Evaporation coefficient for the sea surface from eddy flux measurements. *J. Geophys. Res.* **86**, 449–456.

Atkinson, L. P. 1973. Effect of air bubble solution on air-sea gas exchange. *J. Geophys. Res.* **78**, 962–968.

Broecker, H.-C., Petermann, J. and Siems, W. 1978. The influence of wind on CO_2-exchange in a wind-wave tunnel, including the effects of monolayers. *J. Mar. Res.* **36**, 595–610.

Bortkovskiĭ, R. S. 1987. *Air-sea exchange of heat and moisture during storms.* Dordrecht/Holland: D. Reidel Publ. Comp.

Dawson, D. A. and Trass, O. 1972. Mass transfer at rough surfaces. *Int. J. Heat and Mass Transfer* **15**, 1317–1336.

DeCosmo, J., Katsaros, K. B. and Lind, R. J. 1988. Surface layers measurements during hexmax by the university of Washington. In: *Proceedings of the NATO Advanced Workshop Humidity exchange over the sea: main experiment (HEXMAX), analysis and interpretation* (eds. W. A. Oost, S. D. Smith, and K. B. Katsaros). Dellenhove, Epe, The Netherlands, 29–39.

Donelan, M. A. 1990. Air-sea interaction. In: *The sea: ocean engineering science* (eds. B. Le Méhauté and D. M. Hanes). John Wiley & Sons Inc., 239–292.

Etcheto, J., Boutin, J. and Merlivat, L. 1991. Seasonal variation of the CO_2 exchange coefficient over the global ocean using satellite wind speed measurements. *Tellus* **43B**, 247–255.

Francey, R. J. and Garratt, J. R. 1978. Eddy flux measurements over the ocean and related transfer coefficients. *Boundary-Layer Meteor.* **14**, 153–166.

Garratt, J. R. and Hyson, P. 1975. Vertical fluxes of momentum, sensible heat and water vapor during the air mass transformation experiment (AMTEX) 1974. *J. Meteorol. Soc. Japan* **53**, 149–160.

Hoover, T. E. and Berkshire, D. C. 1969. Effects of hydration on carbon dioxide exchange across an air-water interface. *J. Geophys. Res.* **74**, 456–464.

Jähne, B. 1991. New experimental results on the parameters influencing air-sea gas exchange. In: *Air-water mass transfer* (eds. S. C. Wilhelms and J. S. Gulliver). Am. Soc. Civ. Eng., 582–592.

Jähne, B., Münnich, K. O. and Siegenthaler, U. 1979. Measurements of gas exchange and momentum transfer in a circular wind-water tunnel. *Tellus* **31**, 321–329.

Jähne, B., Huber, W., Dutzi, A., Wais, T. and Ilmberger, J. 1984. Wind/wave-tunnel experiment on the schmidt number, and wave field dependence of air/water exchange. In: *Gas transfer at water surfaces* (eds. W. Brutsaert and G. H. Jirka). D. Reidel Publ. Comp., 303–309.

Jähne, B., Münnich, K. O., Bösinger, R., Dutzi, A., Huber, W. and Libner, P. 1987a. On the parameters influencing air-water gas exchange. *J. Geophys. Res.* **92**, 1937–1949.

Jähne, B., Heinz, G. and Dietrich, W. 1987b. Measurement of the diffusion coefficients of sparingly soluble gases in water. *J. Geophys. Res.* **92**, 10767–10776.

Jähne, B., Libner, P., Fisher, R., Billen, T. and Plate, E. J. 1989. Investigating the transfer process across the free aqueous viscous boundary layer by the controlled flux method. *Tellus* **41B**, 177–195.

Kahma, K. K. and Donelan, M. A. 1988. A laboratory study of the minimum wind speed for wind wave generation. *J. Fluid Mech.* **192**, 339–364.

Kanwisher, J. 1963. On the exchange of gases between the atmosphere and the sea. *Deep-Sea Res.* **10**, 195–207.

Katsaros, K. B. and DeCosmo, J. 1988. The importance of surface flux formulations for numerical models of the atmosphere from global to micro-scale. In: *Proceedings of the NATO Advanced Workshop: Humidity exchange over the sea: main experiment (HEXMAX), analysis and interpretation* (eds. W. A. Oost, S. D. Smith, and K. B. Katsaros). Dellenhove, Epe, The Netherlands, 213–230.

Kitaigorodskii, S. A. 1968. On the calculation of the aerodynamic roughness of the sea surface. *Bull. Acad. Sci. USSR, Atmospheric and Oceanic Physics*, **4**.

Kitaigorodskii, S. A. and Donelan, M. A. 1984. Wind-wave effects on gas transfer. In: *Gas transfer at water surfaces* (eds. W. Brutsaert and G. H. Jirka). D. Reidel Publ. Comp., 147–170.

Large, W. G. and Pond, S. 1982. Sensible and latent heat flux measurements over the ocean. *Jour. Phys. Oceanogr.* **12**, 464–482.

Liss, P. S. 1973. Processes of gas exchange across an air-water interface. *Deep-Sea Res.* **20**, 221–238.

Liss, P. and Merlivat, L. 1986. Air-sea gas exchange rates: introduction and synthesis. In: *Role of air-sea exchange in geochemical cycling* (ed. P. Buat-Ménard). D. Reidel Publ. Comp., 113–127.

Liss, P. S. 1983. Gas transfer: Experiments and Geochemical implications. In: *Air-sea exchange of gases and particles* (eds. P. S. Liss and G. N. Slinn). D. Reidel Publ. Comp., 241–298.

Manahan, S. E. 1984. *Environmental chemistry.* Monterey, California: Brooks/Cole Publ. Comp.

Merzi, N., Servos, M. and Donelan, M. A. 1990. *Description of an air, tight gas transfer flume and an experimental program for mass transfer at the air-water interface.* Technical Report 90-147, National Water Research Institute.

Shaw, D. A. and Hanratty, T. J. 1977. Turbulent mass transfer rates to a wall for large Schmidt numbers. *AIChE J.* **23**, 28–37.

Smith, S. D. 1989. Water vapour flux at the sea surface. *Boundary-Layer Meteorol.* **47**, 277–283.

Smith, S. D. and Anderson, R. J. 1988. Bedford institute of oceanography eddy flux measurements during hexmax. In: *Proceedings of the NATO Advanced Workshop: Humidity exchange over the sea: main experiment (HEXMAX), analysis and interpretation* (eds. W. A. Oost, S. D. Smith, and K. B. Katsaros). Dellenhove, Epe, The Netherlands, 14–21.

Watson, A. J., Upstill-Goddard, R. C. and Liss, P. S. 1991. Air-sea gas exchange in rough and stormy seas measured by a dual-tracer technique. *Nature* **349**, 145–147.

Yin, C. and Hassett, J. P. 1986. Gas-partitioning approach for laboratory and field studies of mirex fugacity in water. *Environ. Sci. Technol.* **20**, 1213–1217.